Carbohydrate Polymers 80 (2010) 687–694

Contents lists available at ScienceDirect

Carbohydrate Polymers

journal homepage: www.elsevier.com/locate/carbpol

Preparation and characterization of chitosan–gelatin/nanohydroxyapatite composite scaffolds for tissue engineering applications

Mathew Peter [a], Nitya Ganesh [a], N. Selvamurugan [a,1], S.V. Nair [a], T. Furuike [b], H. Tamura [b], R. Jayakumar [a,*]

[a] Amrita Centre for Nanosciences and Molecular Medicine, Amrita Institute of Medical Sciences and Research Centre, Amrita Vishwa Vidyapeetham University, Kochi 682 041, India
[b] Faculty of Chemistry, Materials and Bioengineering & High Technology Research Centre, Kansai University, Osaka 564-8680, Japan

ARTICLE INFO

Article history:
Received 29 October 2009
Received in revised form 28 November 2009
Accepted 30 November 2009
Available online 3 December 2009

Keywords:
Chitosan
Gelatin
Nanohydroxyapatite
Composite scaffold
Tissue engineering

ABSTRACT

Chitosan is a novel biocompatible, biodegradable polymer for potential use in tissue engineering. In this work, chitosan–gelatin/nanophase hydroxyapatite composite scaffolds were prepared by blending chitosan and gelatin with nanophase hydroxyapatite (nHA). The prepared nHA was characterized using TEM, XRD and FT-IR. The prepared composite scaffolds were characterized using SEM, FT-IR and XRD studies. The composite scaffolds were highly porous with a pore size of 150–300 μm. In addition, density, swelling ratio, degradation, biomineralization, cytotoxicity and cell attachment of the composite scaffolds were studied. The scaffolds showed good swelling character, which could be modulated by varying ratio of chitosan and gelatin. Composite scaffolds in the presence of nHA showed a decreased degradation rate and increased mineralization in SBF. The biological response of MG-63 cells on nanocomposite scaffolds was superior in terms of improved cell attachment, higher proliferation, and spreading compared to chitosan–gelatin (CG) scaffold.

1. Introduction

The approach of tissue engineering is considered promising to repair or regenerate damaged tissue through the substitution of engineered tissue with the aim that it will help restore the functions during regeneration and subsequent integration with the host tissue. In this regard, significant attention is being given to three-dimensional polymer scaffolds for tissue engineering and drug delivery applications (Shen et al., 2008; Vacanti & Langer, 1999). These scaffolds provide the necessary support as artificial extra cellular matrices, allowing cells to proliferate and maintain their differentiated functions. An ideal scaffold should mimic the natural extracellular environment of the tissue to be regenerated. In bone tissue the extracellular matrix consists of an organic phase made of type I and type III collagen and glycosaminoglycans (GAGs) and an inorganic phase made up of hydroxyapatite (Hutmacher, 2000). Chitosan is a partially deacetylated product made from chitin and is structurally similar to glycosaminoglycans (Muzzarelli, Baldassame, Conti, Ferrara, & Biagini, 1988). Chitosan is biocompatible and can be degraded by enzymes in the human body and the degradation products are non-toxic. Chitosan is widely used in tissue engineering due to its many advantages like hemostasis in wound healing, accelerating tissue regeneration and antibacterial property (Jayakumar, Nwe, Tokura, & Tamura, 2007; Jayakumar, Prabaharan, Reis, & Mano, 2005; Muzzarelli, 2009; Muzzarelli & Giacomelli, 1987; Muzzarelli et al., 1988; Muzzarellii et al., 1990). Chitosan can be moulded into various forms and can form a porous structure by lyophilization (Madihally & Matthew, 1999). However, its bioactivity needs to be improved like most polymers by addition of biologically active materials like hydroxyapatite, collagen or gelatin (Mao, Zhao, Yin, & Yao, 2003).

Gelatin is a partially degraded product of collagen. Collagen has been known to possess antigenicity due to its animal origin; in contrast, gelatin has relatively low antigenicity compared to its precursor, yet it still retains some of the information signals which may promote cell adhesion, differentiation and proliferation, such as the Arg–Gly Asp (RGD) sequence of collagen (Lien, Ko, & Huang, 2009). Gelatin has been blended into chitosan scaffolds to promote cell adhesion, migration, differentiation and proliferation (Nagahama, Divya Rani et al., 2009; Nagahama, Maeda et al., 2009).

Hydroxyapatite (HA) is a major inorganic component of bone. It, is an osteoconductive, non-toxic and non-inflammatory biomaterial, which promotes cell proliferation and osteoblastic cell differentiation (Huang et al., 2004; Manso et al., 2002; Webster, Ergun, Doremus, Siegel, & Bizios, 2000). It has been reported that surface roughness (Degasne et al., 1999; Lauer et al., 2001; Linez-Bataillon, Monchau, Bigerelle, & Hildebrand, 2002), micro and nanotopography (Dalby, Riehle, Johnstone, Affrossman, & Curtis, 2002; Dalby,

* Corresponding author. Tel.: +91 484 2801234; fax: +91 484 2802020.
E-mail addresses: rjayakumar@aims.amrita.edu, jayakumar77@yahoo.com (R. Jayakumar).
[1] Present address: Department of Biotechnology, School of Bioengineering, SRM University, Kattankulathur 603203, India.

0144-8617/$ - see front matter © 2009 Elsevier Ltd. All rights reserved.
doi:10.1016/j.carbpol.2009.11.050

Yarwood et al., 2002; Li et al., 2009) can affect cell morphology, cell spreading, cytoskeletal rearrangement, cell proliferation and differentiation. The size and shape of nHA could play a role in cell viability on composite scaffolds. Scaffolds mimicking the natural extracellular environment could have greater biocompatibility. Previous studies have shown composite scaffolds of chitosan with HA and gelatin improves the biological response of osteoblast cell type (Zhao, Grayson, Ma, Bunnell, & Lu, 2006). However, the influence of nHA in CG composite scaffolds is not well understood. So, in this work, we studied the influence of addition of nHA on the properties of scaffold and also cell viability on the composite scaffold in detail.

2. Experimental

2.1. Materials

Chitosan (degree of deacetylation-85%) was purchased from Koyo Chemical Co. Ltd., (Japan). Gelatin was obtained from Wako chemicals (Japan). Calcium hydroxide, orthophosphoric acid, sodium borohydride, acetic acid, sodium hydroxide, bicinchoninic acid reagent (BCA), Alpha minimum essential medium (α-MEM), 3-(4,5-Dimethylthiazol-2-yl)-2,5-diphenyltetrazolium bromide (MTT), was purchased from Sigma Aldrich. Glutaraldehyde and hen lysozyme was purchased from Fluka. Trypsin–EDTA and fetal bovine serum (FBS) were obtained from Gibco, Invitrogen Corporation.

2.2. Preparation of nanophase hydroxyapatite (nHA)

nHA was synthesized by microwave hydrothermal method (Han, Song, Saito, & Lee, 2006). Briefly, 0.3 M orthophosphoric acid was added to 0.5 M $Ca(OH)_2$ solution drop wise till the pH dropped to 7.4. After that, the solution was transferred into a tightly sealed bottle and micro waved for 8 min and left to cool to room temperature. The resultant precipitate was washed centrifugally with deionized water and ethanol to remove residual precursor. The resultant precipitate was then sintered at 800 °C for 24 h. Following sintering, the resultant HA was powdered using mortar and pestle to reduce size.

2.3. Preparation of composite scaffold

Chitosan 2% (w/v) was dissolved in 1% acetic acid solution. Gelatin was added into chitosan solution and stirred for 12 h at 37 °C. Then nHA (1 wt%) was added to solution and stirred for 24 h to disperse nHA in chitosan solution. Resultant solution was subjected to ultrasonication to further disperse and reduce particle size. 0.25% glutaraldehyde was added as a cross linker. The resultant solution was transferred to 12 well culture plates and pre-freezed at −20 °C for 12 h followed by freeze-drying (Christ alpha LD plus UK) at −80 °C for 48 h. Then scaffolds were neutralized by 2% NaOH and 5% NaBr for 2 h and further washed with deionised water. Then the scaffolds were freeze dried and stored for further use. Three different concentrations (0.5, 1, 2 w/w%) of CG solutions were prepared to which 1% nHA was dispersed and freeze dried to prepare the scaffolds.

2.4. Characterization

2.4.1. FT-IR

FT-IR spectra of nHA and composite scaffolds were obtained using an FT-IR spectrometer Perkin-Elmer RX1 USA. The nHA and composite scaffolds were ground and mixed thoroughly with potassium bromide at a ratio of 1:5 (sample: KBr). The IR spectra of the pellets were then analyzed using Perkin–Elmer RX1 operating at range of 400–4000 cm^{-1}.

2.4.2. XRD

XRD patterns of nHA and composite scaffolds were obtained at room temperature using a Panalytical XPERT PRO, Netherlands powder diffractometer (Cu $K\alpha$ radiation) operating at a voltage of 40 kV. Finely ground scaffold composite materials were analysed in the 2θ angle range of 5–80° and the process parameters were: scan step size 0.02 (2θ) and scan step time 0.05 s.

2.4.3. EDS

Energy-dispersive X-ray spectroscopy (EDS) analysis was performed on JEOL JSM 6490 LA, USA, Japan. A drop of nHA/ethanol was placed on carbon tape coated stub. The sample was then platinum coated with JEOL JFC 1600 for 2 min at 10 mA.

2.4.4. TEM

The image of nHA was taken by diluting nHA powder in ethanol. TEM images were taken using JEOL-JEM2100F, Japan.

2.4.5. SEM

The structural morphology of scaffolds were examined using scanning electron microscope (SEM). Scaffolds were sectioned into thin slices with razor blade. Each sections were placed on aluminium stub and coated with platinum using JEOL JFC 1600, Japan for 2 min at 10 mA before imaging The average pore size was determined by measuring 30 pores and expressed as mean ± S.D. (n = 3).

2.5. Swelling studies

To determine the percentage of water absorption, swelling studies were performed in PBS at pH 7.4 and temperature of 37 °C. The dry weight of the scaffold was noted (W_o). Scaffolds were placed in PBS buffer solution at pH 7.4 and after a predetermined time (24 h) scaffolds were taken out, surface adsorbed water was removed by filter paper and wet weight was recorded (W_w). The ratio of swelling was determined using the following formula:

$$\text{Swelling ratio} = (W_w - W_o)/W_o$$

Swelling ratio was expressed as mean ± S.D. (n = 9).

2.6. Density

To determine the density of scaffold, we selected six scaffolds from each batch and measured using Sartorius analytical balance equipped with density determination kit (Sartorius YDK 01). Density measurements were done with ethanol as the displacement medium. Ethanol did not cause a change in pore size and hence was used as displacement medium. Density was recorded as mean ± S.D. (n = 6).

2.7. In vitro degradation

The degradation of the composite scaffolds were studied in PBS medium containing lysozyme at 37 °C. Three scaffolds were immersed in lysozyme (10,000 U/ml) containing medium and incubated at 37 °C for 7 days. Initial weight of the scaffold was noted as W_o and after 7 days the scaffold was washed in deionised water to remove ions adsorbed on surface and freeze dried. The dry weight was noted as W_t. The degradation of the scaffold was calculated using the following formula:

$$\text{Degradation}\% = (W_o - W_t)/W_o \times 100$$

Degradation rate was recorded as mean ± S.D. (n = 3).

2.8. In vitro biomineralization

Three composite scaffolds of equal weight and shape were immersed in 1× simulated body fluid (SBF) solution and then incubated at 37 °C in a closed Falcon tube for 7 and 14 days. The SBF solution was prepared according to previously reported literature (Kokubo & Takadama, 2006). After specified time, the scaffolds were removed washed three times with deionised water to remove adsorbed minerals. After that, the scaffolds were lyophilized, sectioned and viewed using SEM for mineralization.

2.9. Protein adsorption studies

Scaffolds of same shape and weight were incubated in cell culture media containing 5% FBS for 1 h in 96 well plates. After specific period of time, the scaffolds were rinsed with PBS. For control, deionised water was used as blank. Protein adsorption was assessed using bicinchoninic acid (BCA) assay. BCA reagent was prepared by adding 50 parts of BCA with 1 part of copper (II) sulphate solution. Then BCA reagent was added to each well and incubated for 30 min at 37 °C and OD read at 562 nm. Protein adsorption was plotted as mean ± S.D. ($n = 3$).

2.10. Cell culture studies

Cell studies were conducted using human osteosarcoma cell line (MG-63). Alpha minimum essential medium supplemented with 10% FBS and penicillin–streptomycin was used to culture cells. MG-63 cells with 80–85% confluence were used to seed onto the scaffolds and investigate the cytocompatibility of chitosan and nHA. Prior to cell seeding, the scaffolds were placed in 24-well culture plate and incubated with culture medium for 3 h at 37 °C in a humidified incubator with 5% CO_2. Then, the culture medium was removed from the scaffolds completely. Cells were seeded drop wise onto the top of the scaffolds (1×10^5 cells/scaffold), which fully absorbed the media, allowing cells to distribute throughout the scaffolds. Subsequently, the cell seeded scaffolds were kept at 37 °C in a humidified incubator with 5% CO_2 for 4 h in order to allow the cells to attach to the scaffolds. Next, an additional culture medium was added to cover the scaffolds and incubation was resumed. Fresh medium was replaced every day up to the incubation period.

Cell viability was measured using indirect MTT assay. The assay is based on the reduction of tetrazole by living cells. Cleavage of the tetrazolium rings turns the pale yellow MTT into dark blue formazan crystals, the concentration of which is directly proportional to the number of metabolically active cells. Therefore, the production of formazan can reflect the level of cell viability on the material. This reduction takes place only when mitochondrial reductase enzymes are active. Scaffolds were incubated in culture medium as per ISO specification 10993-5 i.e. 60 cm^2 per 20 ml of medium for 24 h at 37 °C. Then medium with leach able from the scaffold were added to MG-63 cells seeded at density of 10^4 cells in 96 well plate and incubated for 24 and 48 h followed by the addition of 100 μl of MTT. Cells were then incubated for 3 h, followed by solubilization using Triton X-100 to dissolve the intracellular insoluble purple formazan product formed into a coloured solution. The absorbance of this solution was quantified by photospectrometry at 570 nm with a plate reader (BioTEK Instrument). Cells grown without the scaffolds were used as negative control while Triton X-100 was used as positive control. Cell viability was plotted as percentage with respect to negative control ($n = 3$).

Direct contact test was done to show cytocompatability of the composite scaffolds placed in direct contact with cells. Cells were grown to form a monolayer on petri plate and sterilized scaffolds were placed in direct contact with monolayer of cells and incubated for 24 h and 48 h. Cell images were taken with inverted microscope (Leica) fitted with CCD camera and assessed for morphological changes.

Scanning electron microscopy is an appropriate technique to observe spreading pattern, proliferation, and morphology of MG-63 cells. To accomplish this, constructs were fixed with 0.025% glutaraldehyde in PBS buffer pH 7.4, rinsed in PBS, dehydrated in a graded series of ethanol (25–100%). The samples were coated with platinum and examined under SEM.

2.11. Statistical analysis

All quantitative results were obtained from triplicate samples. Data was expressed as the mean ± S.D. Statistical analysis was carried out using Student's two-tailed t test. A p value of < 0.05 was considered to be statistically significant.

3. Results and discussion

3.1. Characterization

3.1.1. FT-IR

FT-IR spectrum of nHA (Fig. 1A) showed peaks at 3571 and 632 cm^{-1}, which corresponds to –OH stretching and bending vibration mode. The band at 473 cm^{-1} corresponds to γ2 of phosphate mode, band at 603 and 571 cm^{-1}corresponds to γ4 of phosphate, 963 cm^{-1} corresponds to γ1 of phosphate and 1045 cm^{-1}corresponds to γ3 of phosphate mode (Han et al., 2006). FT-IR spectrum of CG (Fig. 1) shows a peak at 1649 cm^{-1} corresponds to primary amide groups of chitosan. The peak at 1030 cm^{-1}, which is attributed to phosphate group, was present in CG/nHA scaffold. Peak at

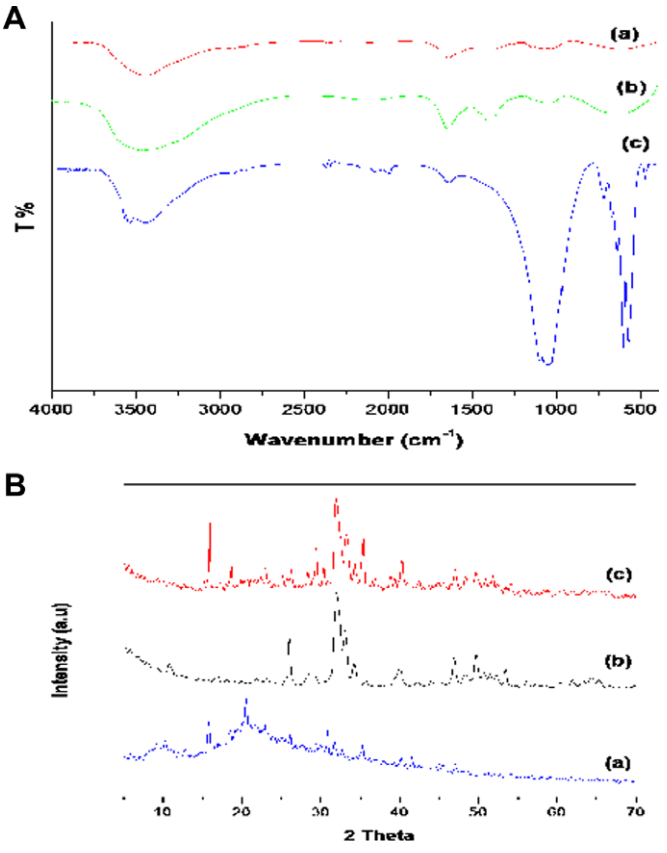

Fig. 1. (A) FT-IR spectra of (a) CG, (b) CG/nHA and (c) nHA, (B) X-ray diffraction patterns of (a) CG, (b) nHA and (c) composite scaffold.

1070 cm^{-1} observed in CG, which was absent in CG/HA which is assigned to C–O stretching of chitosan (Li et al., 2009). Comparing the FT-IR spectrum of CG with CG/nHA (Fig. 1A), suggests that characteristic bands of nHA, chitosan and gelatin are present in the composite scaffolds. In comparison to CG, CG/nHA composite scaffold is characterized by two new absorption bands at 602 and 564 cm^{-1}, corresponding to the stretching vibration bands of P–O from PO_4^{3-}. FT-IR studies show that there was stronger interaction between nHA and CG networks in CG/nHA. The –COOH group of gelatin in the composite scaffold existed in the form of COO^- and the ionic or polar interaction could exist between COO^- and Ca^{2+} and hydrogen bonds could also exist between $-NH_2$ and nHA.

3.1.2. XRD

XRD spectrum of nHA (Fig. 1B) shows diffraction peak at 25.7, 31.7, 32.1, 32.8 and 48.5°. The above peaks also corresponded to (2 1 1) of HA (JCPDS #09-0432) (Han et al., 2006). The XRD of CG/nHA (Fig. 2) scaffold showed peaks at 31.7° attributed to presences of nHA in the composite scaffold, which was absent in CG scaffold. The presence of peak at 21.5° is attributed to gelatin in the scaffold (Thein & Misra, 2009).

3.1.3. TEM

TEM images showed that the particles had a predominantly rod shaped morphology with a particle size being below 100 nm and uniform particle size distribution. The nanoparticles have tendency to aggregate into larger particles (Fig. 2a).

3.1.4. EDS

The EDS spectrum (Fig. 2b) of nHA confirmed the presence of calcium, phosphate and oxygen peaks of nHA. The Ca/P ratio was found to be 1.71. It was near the theoretical value of 1.67. These results indicate a slightly Ca rich apatite.

3.1.5. SEM

The nHA particles coated the walls of the composite scaffold and were uniformly dispersed in the matrix. The pore size of CG and CG/nHA composite scaffold varied from 150–350 μm as measured by SEM (Fig. 3). Although the pore size of CG/HA scaffolds decreased with the addition of nHA compared with CG scaffold the results was not statistically significant. However, with increasing concentration of chitosan the pore size decreased which is in accordance with previously reported literature (Zheng et al., 2007).

3.2. Density

There is a variation in the density, which can be attributed to variation in porosity of the scaffolds. As the concentration of chitosan in the scaffold increases the scaffold density increases and also with the addition of nHA into the scaffolds there was an increase in the density of the composite scaffold (Fig. 4A).

3.3. Swelling studies

Swelling studies CG and CG/nHA composite scaffolds indicated, very high swelling capacity and the ability to retain water more than their original weight (Fig 4B). The addition of nHA decreased the swelling of CG/nHA network (Nordtveit, Varum, & Smidsrod, 1996; Thein & Misra, 2009). This may be due because nHA formed cross-link between the chains and decreased the hydrophilicity of gelatin by binding calcium and phosphate to the hydrophilic –COOH or NH_2 groups. It was also observed that as concentration of chitosan increased the swelling ratio also. Since some of the NH_2 are bound to Ca groups the OH groups cannot form hydrogen bonds, hence the decrease in swelling properties. Moreover, the swelling and degradation of chitosan involves the protonation of amino groups and mechanical relaxation of coiled chitosan chains. Swelling facilitate the cells infiltration into the scaffolds in a three-dimensional fashion, during cell culture. Swelling also increases the pore size and total porosity thus maximizing the internal surface area of the scaffolds. Samples showing higher degree of swelling will have a larger surface area/volume ratio thus allowing the samples to have the maximum probability of cell infusion into the three-dimensional scaffold as well as maximum cell growth by attachment to the scaffold surfaces. The increase in swelling also allows the samples to avail nutrients from culture media more effectively. However, while the swelling of scaffolds would promote cell adhesion it could lower its mechanical properties.

3.4. In vitro degradation studies

Lysozyme is the primary enzyme responsible for *in vivo* degradation of chitosan through hydrolysis of acetylated residues. Other proteolytic enzymes have shown to have low level of degradation activity on the molecule. The degradation rate of chitosan is inversely related to both the degree of crystallinity, and deacetylation. Highly deacetylated forms may thus last several months *in vivo*; eventual degradation products being chitosan oligosaccharides of variable length. The *N*-acetyl glucosamine groups of chitosan chains can be hydrolyzed by lysozyme (Kim, Himeno, Kawashita, Kokubo, & Nakamura, 2004). Its degradation leads to the release of aminosugars, which can be incorporated into glycosaminoglycans and glycoprotein metabolic pathways, or excreted. It is presumed that the macromolecules of the scaffold surface undergo preferential hydrolytic scission into small molecules (oligomeric units), which can dissolve in PBS. The degradation rate of the composite scaffolds was decreased with the addition of nHA into the matrix (Thein & Misra, 2009). Gelatin, being a hydrophilic polymer (presence of amide and carboxyl groups), the macromolecular chains of gelatin polymer hydrolyse quickly in the presence of

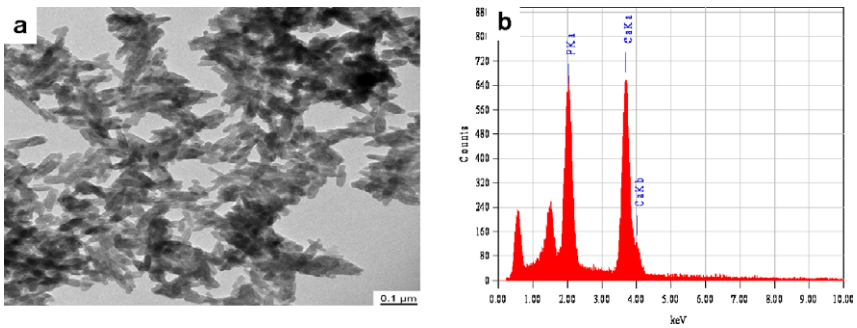

Fig. 2. (a) TEM image of nHA and (b) EDS spectrum of nHA.

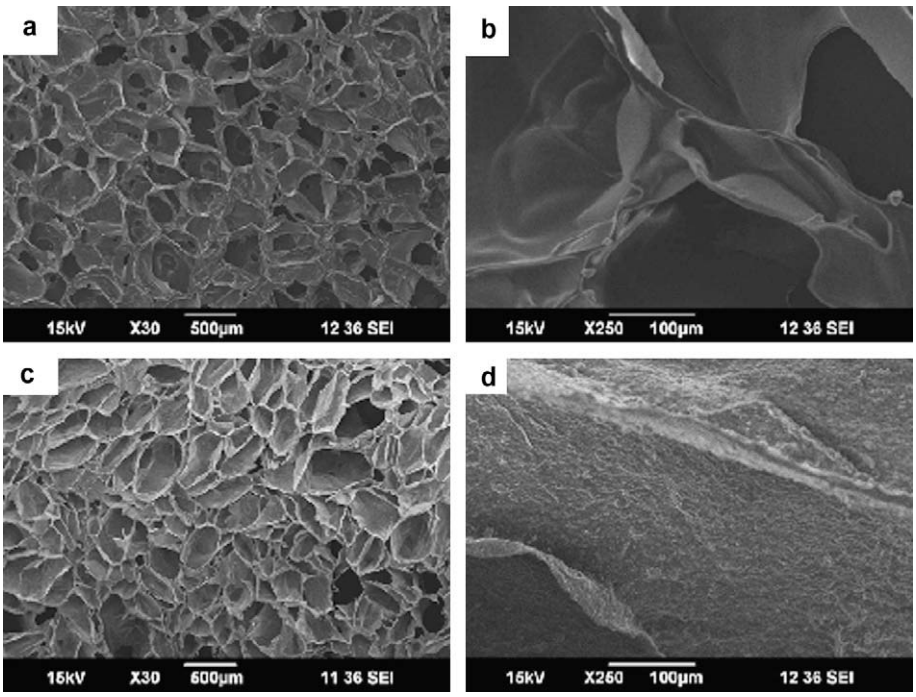

Fig. 3. SEM images of (a) CG and (b) CG/nHA scaffolds.

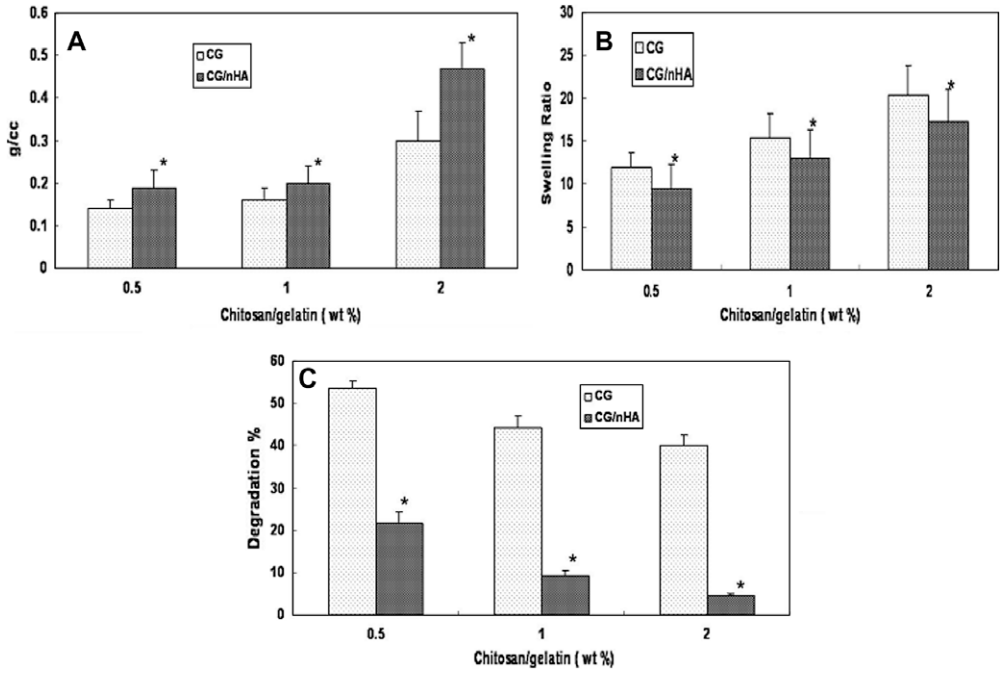

Fig. 4. (A) Density measurements of the scaffolds recorded in ethanol. Density of the scaffolds increased with addition of nHA ($^*p < 0.05$), (B) swelling behaviour of the scaffolds in PBS at 37 °C. Swelling studies show a decrease in swelling ratio with addition of nHA ($^*p < 0.05$) and (C) degradation behaviour of scaffolds in PBS containing lysozyme at 37 °C degradation rate is lower for composite scaffold ($^*p < 0.05$).

water. The degradation rate of the composite scaffolds with high gelatin concentration was higher in lysozyme solution (Marques & Reis, 2005). In the presence of nHA the degradation rate of the composite scaffold was substantially decreased (Fig. 4C) as reported earlier, by reducing the accessibility of enzymes to the attacking sites in polysaccharide molecules (Marques & Reis, 2005). This shows that the degradation of the composite scaffold can be modified by changing the gelatin concentration or by addition of nHA.

3.5. In vitro biomineralization studies

The scaffolds showed excellent ability to undergo mineralization in SBF solution at physiological pH and temperature (Fig. 5A). The morphology of apatite deposition changed after 14 days incubation. After 7 days of incubation in 1× SBF, minerals were seen to deposit on the surface of the scaffold. However, after 14 days the deposits were seen to coat the surface of the pore. FT-IR studies (Fig. 5B) show that the phosphate peaks at 603 and

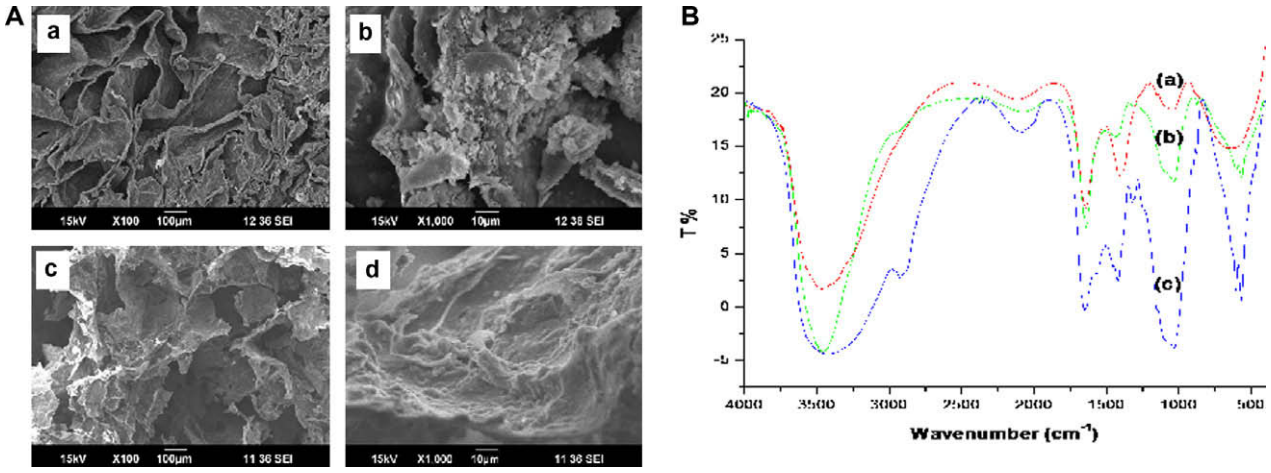

Fig. 5. (A) SEM image shows the mineralization of the composite scaffolds immersed in SBF after (a and b) 7 and (c and d) 14 days incubation at different magnifications and (B) FT-IR spectrum of the composite scaffolds immersed in SBF solution after (a) 0 (control) (b) 7 and (c) 14 days.

567 cm^{-1} increased in intensity with sharpening of the peaks (Madhumathi et al., 2009; Maeda, Jayakumar, Nagahama, Furuike, & Tamura, 2008). This result suggests that the mineral deposition increases with increasing time. This result may be due to the fact that nHA decreases the surface energy for nucleation of minerals on the surface of the scaffolds. SBF is a metastable calcium phosphate solution supersaturated with respect to apatite. It is reported that the barrier for homogeneous nucleation of apatite is too high and a stimulus is required to induce the heterogeneous nucleation of apatite from the SBF. On the composite scaffolds there were many nHA particles, which could act as nucleation sites. As a result, apatite could be formed more efficiently on the composite scaffolds than on the CG scaffolds. Therefore, in the same interval of time, more apatite was deposited on the composite scaffolds than the CG scaffolds. It has been reported that the formation of apatite on artificial materials is induced by functional groups, having negative charge, which further induce apatite via the formation of amorphous calcium phosphate (Marques & Reis, 2005). The more nHA content in the composite scaffolds, more will be the nucleation initiation sites and negative charge will exist; as a result more apatite will be formed. Once the apatite nuclei are formed, they can grow spontaneously by consuming the calcium and phosphate ions present in the surrounding fluid. The present results indicated that the addition of nHA enhanced the bioactivity of the CG scaffolds.

3.6. Protein adsorption studies

The protein adsorption of the composite scaffolds incubated in culture media after 1 h were assessed by BCA assay. BCA is used as the detection reagent for Cu^{1+}, which is formed when Cu^{2+} is reduced by protein in an alkaline environment. The purple coloured reaction product is formed by the chelation of two molecules of BCA with one cuprous ion (Cu^{1+}). This water-soluble complex exhibits a strong absorbance at 562 nm that is linear with increasing protein concentration. The incorporation of nHA into the

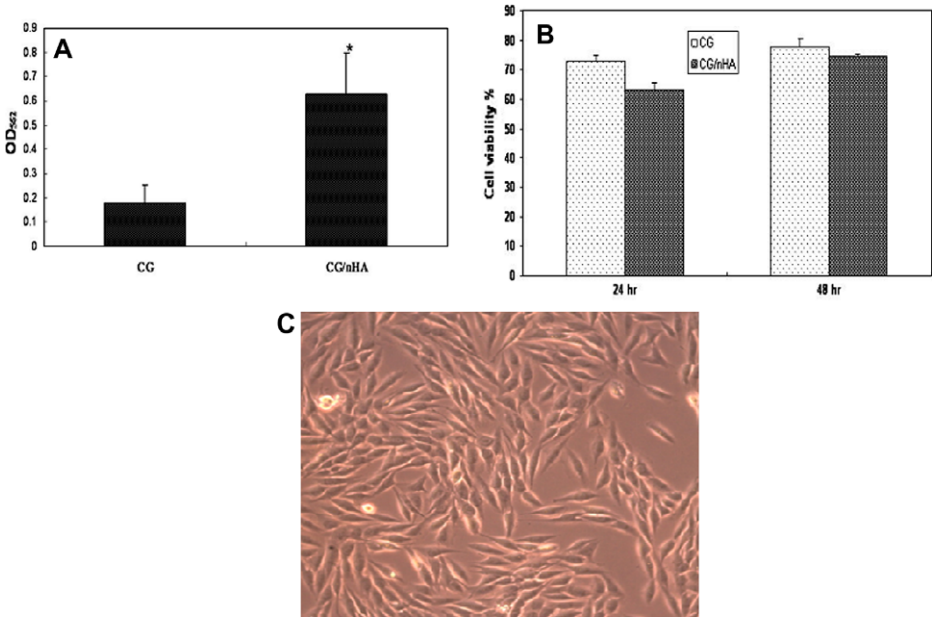

Fig. 6. (A) Protein adsorption on the scaffolds incubated with culture media for 1 h. Total protein adsorption was significantly high on composite scaffold. (*$p < 0.05$), (B) the cell viability of CG/nHA composite scaffolds was assessed by direct MTT assay and (C) morphology of MG-63 cells which were grown after direct contact with the composite scaffolds.

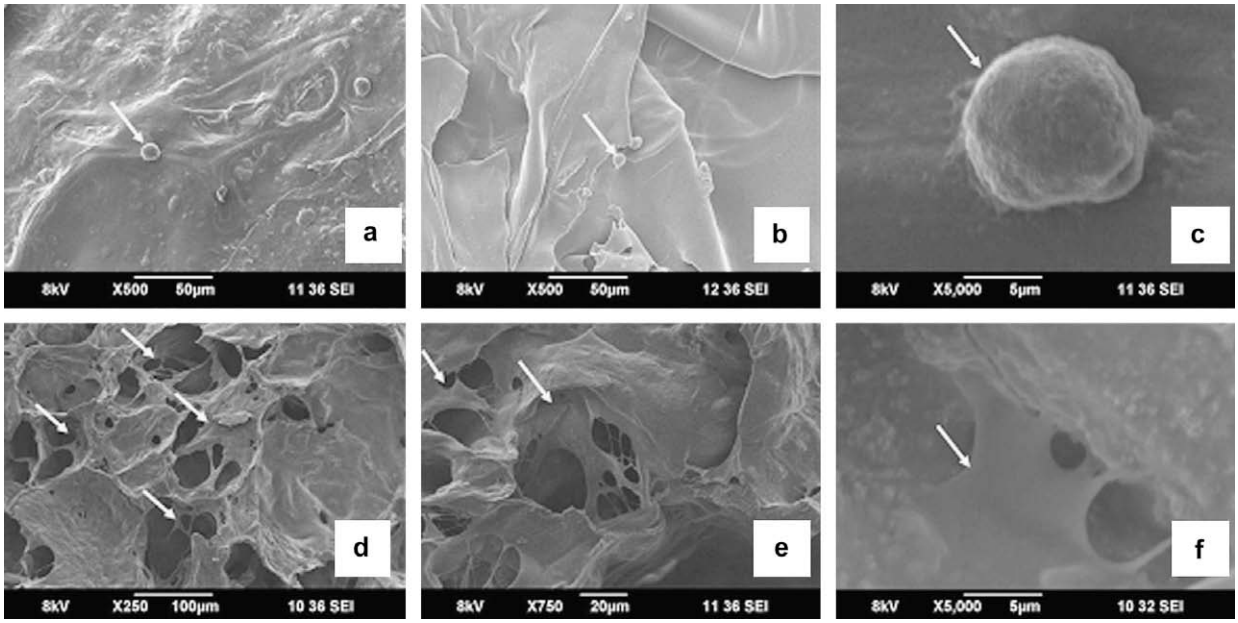

Fig. 7. SEM images showing MG-63 cells attached on the (a–c) CG and (d–f), CG/nHA composite scaffolds. Arrow shows the cells that have adhered to scaffolds.

scaffolds improved the protein adsorption property of the CG polymer network (Fig. 6A) and formed a microenvironment on the scaffold surface rich in protein (Kilpadi, Chang, & Bellis, 2001). One possible explanation to this could be the increase in surface area due to the incorporation of nanoparticles on surface of the pore. The exposed nHA on the composite scaffold surfaces may increase the binding sites of the material surface for proteins or enforce the electrostatic interaction between the proteins and material surface and enhance adsorption of proteins. HA surfaces are known to passively adsorb RGD peptides, which can increase the adhesion of cells (Chou, Marek, & Wagner, 1999; Sawyer, Hennessy, & Bellisa, 2005).

3.7. Cell viability studies

MTT results show that composite scaffolds showed a slightly decreased OD value after 24 h, however after 48 h no significant difference was seen compared to CG scaffold (Fig. 6B). This could be due to the low crystallinity of nHA will leads to dissolution of calcium and phosphate into the media which in turn leads to increase in intracellular Ca and phosphate concentration which may induce cell death (Chou et al., 1999). Both the scaffolds supported 65–70% cell viability compared to the control. Direct contact test was then done to assess the cytocompatability of the composite scaffolds when placed in direct contact with cells. The results show that the composite scaffolds are cytocompatible and no morphological change was observed in MG-63 cells placed in direct contact with composite scaffold (Fig. 6C).

3.8. Cell morphology on scaffolds

Cell adhesion studies also showed that the cells were attached to the scaffold and spread to occupy the pore walls after 48 h in culture. In CG scaffolds, we observed only few cells and cell morphology was rounded in the same period of time (Fig. 7a–c). In the case CG/nHA composite scaffolds we found substantial cell attachment and spreading (Fig. 7d–f). The morphology of the cells were flattened, sheet like with filopodial extension was seen in SEM image. Clearly the nHA improved the formation of focal adhesion and allowed for substantial cell spreading. This is quite likely related to the enhanced protein adsorption on the surface in the presence of nHA. The results indicate that the CG/nHA composite scaffolds were superior to CG scaffolds for tissue engineering applications.

4. Conclusions

Three-dimensional CG/nHA composite scaffolds were prepared, characterized and compared with corresponding CG scaffolds. The composite scaffold was macro porous in nature with pore size varying from 150–300 µm. The mechanical and biological properties of the scaffolds were significantly affected by addition of nHA and by changing the ratio of chitosan and gelatin in the scaffold. Gelatin decreased the density and increased the extent of biodegradability. When nHA was added to CG scaffolds, density was increased and biodegradability decreased with no statistical change in pore size. The increase in density was related to a decrease in swelling and a decrease in total porosity. nHA substantially improved protein adsorption and cell attachment on the internal scaffold surfaces. Thus nHA played the role of improving biological and mechanical properties of the scaffolds at the same time. The addition of nHA to CG scaffolds provided a more promising scaffold for tissue engineering applications.

Acknowledgments

The Department of Science and Technology, Government of India supported this work, under a centre grant of the Nanoscience and Nanotechnology Initiative program monitored by Dr. C.N.R. Rao. The authors are thankful to Prof. Greta R. Patzke, Institute of Inorganic Chemistry, University of Zurich for helping in TEM studies. The authors are also thankful to Mr. Sajin. P. Ravi for helping in SEM studies.

References

Chou, L., Marek, B., & Wagner, W. R. (1999). Effects of hydroxylapatite coating crystallinity on biosolubility, cell attachment efficiency and proliferation *in vitro*. *Biomaterials, 20*, 977–985.

Dalby, M. J., Riehle, M. O., Johnstone, H. J. H., Affrossman, S., & Curtis, A. S. G. (2002). Polymer-demixed nanotopography: Control of fibroblast spreading and proliferation. *Tissue Engineering, 8*, 1099–1108.

Dalby, M. J., Yarwood, S. J., Riehle, M. O., Johnstone, H. J., Affrossman, S., & Curtis, A. S. (2002). Increasing fibroblast response to materials using nanotopography: Morphological and genetic measurements of cell response to 13-nm-high polymer demixed islands. *Experimental Cell Research, 276*, 1–9.

Degasne, I., Basle, M. F., Demais, V., Hure, G., Lesourd, M., Grolleau, B., et al. (1999). Effects of roughness, fibronectin and vitronectin on attachment, spreading, and proliferation of human osteoblast-like cells (Saos-2) on titanium surfaces. *Calcified Tissue International, 64*, 499–507.

Han, J. K., Song, H. Y., Saito, F., & Lee, B. T. (2006). Synthesis of high purity nano-sized hydroxyapatite powder by microwave-hydrothermal method. *Material Chemistry and Physics, 99*, 235–239.

Huang, J., Best, S. M., Bonfield, W., Brooks, R. A., Rushton, N., Jayasinghe, S. N., et al. (2004). In vitro assessment of the biological response to nano-sized hydroxyapatite. *Journal of Material Science, Materials in Medicine, 15*, 441–445.

Hutmacher, D. W. (2000). Scaffolds in tissue engineering of bone and cartilage. *Biomaterials, 21*, 2529–2543.

Jayakumar, R., Nwe, N., Tokura, S., & Tamura, H. (2007). Sulfated chitin and chitosan as novel biomaterials. *International Journal of Biological Macromolecules, 40*, 175–181.

Jayakumar, R., Prabaharan, M., Reis, R. L., & Mano, J. F. (2005). Graft copolymerized chitosan-present status and applications. *Carbohydrate Polymers, 62*, 142–158.

Kilpadi, K. L., Chang, P. L., & Bellis, S. L. (2001). Hydroxyapatite binds more serum proteins, purified integrins, and osteoblast precursor cells than titanium or steel. *Journal of Biomedical Material Research, 57*, 258–267.

Kim, H. M., Himeno, T., Kawashita, M., Kokubo, T., & Nakamura, T. (2004). The mechanism of biomineralization of bone-like apatite on synthetic hydroxyapatite: An in vitro assessment. *Journal of the Royal Society Interface, 1*, 17–22.

Kokubo, T., & Takadama, H. (2006). How useful is SBF in predicting in-vivo bone activity? *Biomaterials, 27*, 2907–2915.

Lauer, G., Wiedmann-Al-Ahmad, M., Otten, J. E., Hubner, U., Schmelzeisen, R., & Schilli, W. (2001). The titanium surface texture effects adherence and growth of human gingival keratinocytes and human maxillar osteoblast-like cells in vitro. *Biomaterials, 22*, 2799–2809.

Li, J., Dou, Y., Yang, J., Yin, Y., Zhang, H., Yao, F., et al. (2009). Surface characterization and biocompatibility of micro and nano hydroxyapatite/chitosan–gelatin network films. *Material Science Engineering-C, 29*, 1207–1215.

Lien, S. M., Ko, L. Y., & Huang, T. J. (2009). Effect of pore size on ECM secretion and cell growth in gelatin scaffold for articular cartilage tissue engineering. *Acta Biomaterialia, 5*, 670–679.

Linez-Bataillon, P., Monchau, F., Bigerelle, M., & Hildebrand, H. F. (2002). In vitro MC3T 3 osteoblast adhesion with respect to surface roughness of Ti6A14 V substrates. *Biomolecular Engineering, 19*, 133–141.

Madhumathi, K., Binulal, N. S., Nagahama, H., Tamura, H., Shalumon, K. T., Selvamurugan, N., et al. (2009a). Preparation and characterization of novel (-chitin–hydroxyapatite composite membranes for tissue engineering applications. *International Journal of Biological Macromolecules, 44*, 1–5.

Madihally, S. V., & Matthew, H. W. (1999). Porous chitosan scaffolds for tissue engineering. *Biomaterials, 20*, 1133–1142.

Maeda, Y., Jayakumar, R., Nagahama, H., Furuike, T., & Tamura, H. (2008). Synthesis, characterization and bioactivity studies of novel β-chitin scaffolds for tissue-engineering applications. *International Journal of Biological Macromolecules, 42*, 463–467.

Manso, M., Ogueta, S., Fernandez, P. H., Vazquezl, L., Langlet, M., & Ruiz, J. P. G. (2002). Biological evaluation of aerosol-gel-derived hydroxyapatite coatings with human mesenchymal stem cells. *Biomaterials, 23*, 3985–3990.

Mao, J. S., Zhao, L. G., Yin, Y. J., & Yao, K. D. (2003). Structure and properties of bilayer chitosan–gelatin scaffolds. *Biomaterials, 24*, 1067–1074.

Marques, A. P., & Reis, R. L. (2005). Hydroxyapatite reinforcement of different starch-based polymers affects osteoblast-like cells adhesion/spreading and proliferation. *Material Science and Engineering-C, 25*, 215–229.

Muzzarelli, R. A. A. (2009). Chitins and chitosans for the repair of wounded skin, nerve, cartilage and bone. *Carbohydrate Polymers, 76*, 167–182.

Muzzarelli, R., Baldassame, V., Conti, F., Ferrara, P., & Biagini, G. (1988). Biological activity of chitosan: Ultrastructural study. *Biomaterials, 9*, 247–252.

Muzzarelli, R. A. A., & Giacomelli, G. (1987). The blood anticoagulant activity of *N*-carboxymethyl chitosan trisulfate. *Carbohydrate Polymers, 7*, 87–96.

Muzzarellii, R. A. A., Tarsi, R., Filippini, O., Giovanetti, E., Biagini, G., & Varaldo, P. E. (1990). Antimicrobial properties of *N*-carboxybutyl chitosan. *Antimicrobial Agents and Chemotherapy, 34*, 2019–2023.

Nagahama, H., Divya Rani, V. V., Shalumon, K. T., Jayakumar, R., Nair, S. V., Koiwa, S., et al. (2009). Preparation, characterization, bioactive and cell attachment studies of α-chitin/gelatin composite membranes. *International Journal of Biological Macromolecules, 44*, 333–337.

Nagahama, H., Maeda, H., Kashiki, T., Jayakumar, R., Furuike, F., & Tamura, H. (2009). Preparation and characterization of novel chitosan/gelatin membranes using chitosan hydrogel. *Carbohydrate Polymers, 76*, 255–260.

Nordtveit, R. J., Varum, K. M., & Smidsrod, O. (1996). Degradation of partially *N*-acetylated chitosans with hen egg white and human lysozyme. *Carbohydrate Polymers, 29*, 163–167.

Sawyer, A. A., Hennessy, K. M., & Bellisa, S. L. (2005). Regulation of mesenchymal stem cell attachment and spreading on hydroxyapatite by RGD peptides and adsorbed serum proteins. *Biomaterials, 26*, 1467–1475.

Shen, Y., Zhan, Y., Tang, J., Xu, P., Johnson, P. A., Radosz, M., et al. (2008). Multifunctioning pH-responsive nanoparticle from hierarchical self-assembly of polymer brush for cancer drug delivery. *AIChE Journal, 54*, 2979–2989.

Thein, H. W. W., & Misra, R. D. K. (2009). Biomimetic chitosan–nanohydroxyapatite composite scaffolds for bone tissue engineering. *Acta Biomaterialia, 5*, 1182–1197.

Vacanti, J. P., & Langer, R. (1999). Tissue engineering: The design and fabrication of living replacement devices for surgical reconstruction and transplantation. *Lancet, 354*, 32–34.

Webster, T. J., Ergun, C., Doremus, R. H., Siegel, R. W., & Bizios, R. (2000). Enhanced functions of osteoblasts on nanophase ceramics. *Biomaterials, 21*, 1803–1810.

Zhao, F., Grayson, W. L., Ma, T., Bunnell, B., & Lu, W. W. (2006). Effects of hydroxyapatite in 3-D chitosan–gelatin polymer network on human mesenchymal stem cell construct development. *Biomaterials, 27*, 1859–1867.

Zheng, J. P., Wang, C. Z., Wang, X. X., Wang, H. Y., Zhuang, H., & Yao, K. D. (2007). Preparation of biomimetic three-dimensional gelatin/montmorillonite–chitosan scaffold for tissue engineering. *Reactive and Functional Polymers, 67*, 780–788.